remote sensing

MDPI

Article

Galileo Augmenting GPS Single-Frequency Single-Epoch Precise Positioning with Baseline Constrain for Bridge Dynamic Monitoring

Qiuzhao Zhang [1,2,3], Chun Ma [2,*], Xiaolin Meng [3,4,*], Yilin Xie [3,4], Panagiotis Psimoulis [4], Laiyi Wu [5], Qing Yue [5] and Xinjun Dai [5]

1 NASG Key Laboratory of Land Environment and Disaster Monitoring, China University of Mining and Technology, Xuzhou 221116, China; qiuzhaocumt@cumt.edu.cn
2 School of Environment Science and Spatial Informatics, China University of Mining and Technology, Xuzhou 221116, China
3 Sino-UK Geospatial Engineering Centre, University of Nottingham, Nottingham NG7 2TU, UK; yilin.xie@nottingham.ac.uk
4 Nottingham Geospatial Institute, University of Nottingham, Nottingham NG7 2TU, UK; panagiotis.psimoulis@nottingham.ac.uk
5 China Railway Major Bridge (Nanjing) Bridge and Tunnel Inspect & Retrofit Co., LTD, Nanjing 210000, China; wuly@brdi.com.cn (L.W.); yueq@brdi.com.cn (Q.Y.); daixj@brdi.com.cn (X.D.)
* Correspondence: machun310@cumt.edu.cn (C.M.); xiaolin.meng@nottingham.ac.uk (X.M.); Tel.: +86-187-9622-5453 (C.M.); +44-(0)-0115-84-66029 (X.M.)

Received: 14 January 2019; Accepted: 17 February 2019; Published: 20 February 2019

Abstract: The Single-frequency Single-epoch double-differenced baseline resolution technique of Global Positioning System (GPS) provides a good opportunity for monitoring the displacement or deflection behavior of bridges under different loading conditions in real-time. However, for single GPS, a high success rate baseline solution is difficult to achieve due to the lack of sufficient visible satellites and the low accuracy of float solutions. Galileo Satellite Navigation System (Galileo) has 14 medium earth orbit satellites (as of May 2018) that can be used to supplement GPS. The frequency bands of Galileo overlap with that of GPS on E1/L1 and E5a/L5, which is conducive to the combination of observations in integration positioning. Accordingly, Galileo augmenting GPS is an effective and necessary approach to improve the positioning availability and reliability. Moreover, using the baseline length constraint can improve the accuracy of float solutions, narrow the search space, and finally increase the success rate of ambiguity resolution and positioning. The single-frequency single-epoch double-differenced GPS/Galileo mathematical model with baseline length constraint is deduced in this paper. Two sets of GNSS real bridge data were used for further analysis on the improvement of GPS/Galileo with baseline length constraint when compared to single GPS. Finally, a Fast Fourier Transformation (FFT) algorithm was adopted for precisely detecting the local dominant frequencies of XB, YB, and ZB direction of the two stations.

Keywords: bridge dynamic monitoring; Galileo; GPS; baseline length constraint

1. Introduction

The global positioning system (GPS) technology exhibits several advantages, such as easy to obtain absolute position solution, weather independence, autonomous operation, and not requiring a line-of-sight between target points [1]. This provides a great opportunity for the monitoring of displacement or deflection of bridges under different loading conditions in real time. Recent studies have demonstrated the feasibility of deploying GPS receivers as 'smart sensors' for the dynamic

monitoring of bridges [2]. Roberts and Meng et al. are the early researchers that used integrated GPS and accelerometers to monitor the deflection of bridges [3,4]. Psimoulis et al. found that GPS is suitable in the identification of dynamic characteristics of even relatively rigid (modal frequencies up to 4 Hz) civil engineering structures that are excited by various loads (wind, traffic, earthquakes, etc.) if the displacements are less than the uncertainty level of the method (such as 5 mm) [5]. Efforts have been made in recent years in the use of an integrated monitoring system that consists of dual frequency GPS or Global Navigation Satellite System (GNSS) receivers and triaxial accelerometers for the detection of the dynamics of long span road bridges [6,7]. Recently, bridge monitoring was implemented using the BeiDou Satellite Navigation System (BDS)-Real-Time Kinematic (RTK) and GPS-RTK techniques [8].

Although high accuracy demanding users can typically observe an average number of 8–10 GPS satellites, actually, in several moments of one day, the number of available satellites may decrease to 4–6 or many such satellites are low-elevation ones. In these cases, GPS constellation cannot maintain high-accuracy in a single-frequency single-epoch (SFSE) positioning model [9]. Accordingly, the application of a multi-GNSS system can significantly improve the positioning performance. Shi et al. demonstrated that the positioning performance of BDS in the Asia-Pacific region is comparable to that of GPS [10]. The Quasi-Zenith Satellite System (QZSS) has been operated as a four-satellite constellation since November 2018, and three satellites can be available at all times to users in the Asia-Oceania region. Hence, both the QZSS and BDS systems can be used to improve the performance of GPS positioning in the above regions [11]. However, for European users, the Galileo Satellite Navigation System (Galileo) can only be used to improve the robustness and accuracy of GPS precise positioning. By launching the first four Galileo satellites in pairs, on 21 October 2011 and 12 October 2012, the Galileo system successfully concluded the In-Orbit Validation (IOV) phase at the end of 2013. Currently, Galileo has 23 satellites in the operational orbits and all transmit data on three carrier frequencies (http://esamultimedia.esa.int/docs/Galileo). In addition, it is stated on the Galileo website that initial services were made available by the end of 2016 and system completion is scheduled for 2020 [12]. A project, named GEO6, was oriented to define and implement new applications of Galileo. As such an example, the GNSS and Earth Observation for Structural Health Monitoring (GeoSHM) system, which is funded by the European Space Agency, is a project that applies GNSS (including Galileo) and Earth Observation techniques to monitoring bridge deformation [7].

Since the plan for the Galileo satellites was proposed, the potential benefits of the single Galileo or integrated Galileo/GPS navigation system have been explored. The two key required navigation performance (RNP) parameters, i.e., accuracy and integrity, were addressed in detail. The results showed significant improvements in accuracy and integrity when a integrated constellation is used rather than Galileo alone [13]. The Position Dilution of Precision (PDOP) simulation showed that the mean PDOP values of the integrated GPS/Galileo system are better than that of only GPS [14]. Another simulation result revealed that, given the positioning accuracy, the horizontal positioning availability of GALILEO is comparable to that of GPS, but its vertical positioning availability performs better [15]. The performance of GPS/Galileo was evaluated through simulation in terms of global availability, accuracy, and reliability [16]. The performance of a GPS/Galileo network-based real-time kinematic was evaluated by assessing the success rates of correct integer ambiguity resolution with simulation software [17].

With the launch of Galileo in-orbit validation (IOV) satellites, more work was conducted to evaluate the performance of Galileo and GPS/Galileo using real data. The performance of the Galileo IOV satellites was evaluated with respect to carrier-to-noise density ratio (C/N0), pseudo-range multipath, Galileo broadcast satellite orbit and single point positioning (SPP) accuracy in Galileo-only mode, as well as in integrated GPS/Galileo mode [18]. Several strategies that are based on the processing of dual-frequency GPS, multi-frequency Galileo, and tightly combined GPS/Galileo signals were tested and analyzed for their applicability for long-range precise instantaneous positioning [19]. It is shown that the current accuracy level of daily baseline solutions can be improved by using the additional Galileo constellation for high precision long baseline [20]. The ambiguity resolution

success rate of GPS/Galileo for a 250 km baseline that is based on the ambiguity variance matrix was predicted and it was concluded that ambiguity resolution will likely become faster (less than ten minutes) in the case of integrated GPS/Galileo when based on triple frequency data of both systems [21]. The performance of several precise point positioning (PPP) models, combining dual-frequency GPS/Galileo observations in the un-differenced and between-satellite single-difference (BSSD) modes, was compared. It is shown that the traditional un-differenced GPS/Galileo PPP model, the GPS decoupled clock model, and the semi-decoupled clock GPS/Galileo PPP model improve the convergence time by about 25% in comparison with the un-differenced GPS-only model [22]. The contribution of Galileo satellite data to GNSS solutions for short and long baselines was also evaluated. When compared to GPS, GLONASS, and all solutions, the Galileo results vary greatly. When the Galileo observations are combined with other observations, the precision goes down [12]. The real time positioning results using signals from Galileo satellites only were presented. 14 Galileo satellites were used and the number of simultaneously observed Galileo satellites varied from five to seven. The tests results showed that it is possible to infer the current availability, continuity, convergence time, and accuracy of the RTK measurements [23]. Besides, there is some research that focuses on the applications of GPS/Galileo differential inter-system biases (DISBs) [24–26] and GPS/Galileo/BDS/QZSS RTK [27,28].

Some literature only analyzed the Galileo positioning performance based on simulation results, while other work examined the GPS/Galileo or GPS/Galileo/BDS/QZSS data sets that were gathered from stationary stations. These results could not comprehensively reflect the current features of the Galileo constellation and its enhancement effect on GPS for dynamic situation, such as for bridge monitoring. Since dual frequency GNSS receivers are very expensive (around at least $10,000 per unit) for many engineering applications, the SFSE double-differenced (DD) baseline resolution became the most frequently used method for achieving high-accuracy positioning [29]. Accordingly, the performance of the SFSE carrier phase DD baseline resolution for the integrated GPS/Galileo needs more attention, especially for the deformation monitoring of large structures.

In this paper, the effect of Galileo augmenting GPS was analyzed from the availability, PDOP, ambiguity dilution of precision (ADOP), and success rate for bridge monitoring. The enhancement effects of Galileo and the baseline length constraint on bridge monitoring were emphatically studied. This paper is arranged as follows: Section 1 is the introduction. The SFSE double-differenced GPS/Galileo mathematical model with baseline length constraint is derived in Section 2. Section 3 introduces the bridge monitoring data collection and the corresponding satellite availability and PDOP are analyzed. Section 4 mainly includes the calculation and analysis of the two sets of bridge baseline data. The performance of integrated GPS/Galileo precision positioning with baseline length constraints for bridge monitoring is evaluated with different indicators, and the frequency analysis of bridge vibration is also performed. Finally, the main conclusions are drawn in Section 5.

2. SFSE Double-Differenced GPS/Galileo Mathematical Model

This section mainly discusses the SFSE double-differenced mathematical models for integrated GPS/Galileo relative positioning, including the non-differenced and double-differenced code and phase observation equations for single system and DD equations for integrated systems with different combination strategies with/without DISBs. Finally, the baseline length constraint model and the corresponding stochastic model are deduced.

2.1. Single GPS/Galileo Code and Phase Observation Equations

GPS satellites broadcast their position and clock information in GPS Time (GPST), while Galileo satellites work in an independent time system, that is, Galileo System Time (GST). Therefore, it is a prerequisite to unify the time system before the GPS/Galileo dual constellations are used in positioning, navigation, and timing (PNT) service. Assume that both GPS and Galileo code and phase observations are formed in the same time system-GPST; hence, a GPS-to-Galileo Time Offset (GGTO) [30] needs to

be adopted to convert the transmission epoch of the Galileo satellite to GPST. Subsequently, the SFSE non-differenced code and phase equations for the receiver b and GPS satellite g at frequency j can be expressed as [24].

$$\begin{aligned} P_{b,j}^{g} &= \rho_{b}^{g} - c \cdot \delta t_{b} + c \cdot \delta t^{g} + d_{b,j}^{G} - d_{,j}^{g} + I_{b,j}^{g} + T_{b,j}^{g} + \varepsilon_{b,j}^{g} \\ \lambda_{j} \cdot \phi_{b,j}^{g} &= \rho_{b}^{g} - c \cdot \delta t_{b} + c \cdot \delta t^{g} + \lambda_{j}\left(\delta_{b,j}^{G} - \delta_{,j}^{g} + N_{b,j}^{g}\right) - I_{b,j}^{g} + T_{b,j}^{g} + \in_{b,j}^{g} \end{aligned} \tag{1}$$

where $P_{b,j}^{g}$ and $\phi_{b,j}^{g}$ are the GPS code observation (m) and phase observation (cycle), respectively; ρ_{b}^{g} denotes the real range (m) between the receiver and the GPS satellite; λ_j is the wavelength (m) of the frequency j; δt_b and δt^g are the receiver clock error (s) and GPS satellite clock error (s), respectively; c is the velocity of light (m/s); $d_{b,j}^{G}$ and $\delta_{b,j}^{G}$ are the hardware GPS code delay (m) and phase delay (cycle) in the receiver, respectively, and the superscript "G" represents "GPS"; $d_{,j}^{g}$ and $\delta_{,j}^{g}$ are the hardware code delay (m) and phase delay (cycle) in the GPS satellite; $N_{b,j}^{g}$ denotes the unknown integer ambiguities (cycle); $I_{b,j}^{g}$ and $T_{b,j}^{g}$ denote the ionospheric delay (m) and tropospheric delay (m), respectively; and, $\varepsilon_{b,j}^{g}$ and $\in_{b,j}^{g}$ are the other unmodeled errors (m) of the code and phase equations, including multipath error, random noise, etc.

Because the frequency bands of the Galileo system overlap with those of GPS in L1/E1 and L5/E5a, the frequency of Galileo is still denoted by the subscript "j". To distinguish from the GPS satellite, the Galileo satellite is expressed by the superscript "e". Subsequently, the SFSE non-differenced code and phase equations for Galileo satellites at frequency j can read as:

$$\begin{aligned} P_{b,j}^{e} &= \rho_{b}^{e} - c \cdot \delta t_{b} + c \cdot \delta t^{e} + d_{b,j}^{E} - d_{,j}^{e} + I_{b,j}^{e} + T_{b,j}^{e} - GGTO + \varepsilon_{b,j}^{e} \\ \lambda_{j} \cdot \phi_{b,j}^{e} &= \rho_{b}^{e} - c \cdot \delta t_{b} + c \cdot \delta t^{e} + \lambda_{j}\left(\delta_{b,j}^{E} - \delta_{,j}^{e} + N_{b,j}^{e}\right) - I_{b,j}^{e} + T_{b,j}^{e} - GGTO + \in_{b,j}^{g} \end{aligned} \tag{2}$$

where GGTO denotes the time offset between GPST and GST. It is clearly revealed in (2) that the Galileo code and phase non-differenced observation equations are very similar to those of GPS, with the only difference being the GGTO.

To eliminate the satellite-specific biases (satellite clock error, ionospheric delay, tropospheric delay, and satellite code and phase delay) and receiver-specific biases (receiver clock error, receiver code, and phase delay) and to simplify the observation equations, the double-differenced technique relative to the observations of a base receiver (denoted using subscript b, the rover receiver is denoted using subscript r) and a pivot receiver (denoted using superscript 1G for GPS and 1E for Galileo, the other satellites are denoted while using superscript g and e, respectively) is usually applied in equation construction. Moreover, the system time deviation item GGTO in Galileo observation equations is also offset. Subsequently, the single GPS/Galileo SFSE code and phase double-differenced equations can be expressed as:

$$\begin{aligned} \nabla\Delta P_{br,j}^{1G,g} &= \nabla\Delta\rho_{br}^{1G,g} + \nabla\Delta\varepsilon_{br,j}^{1G,g} \\ \lambda_{j} \cdot \nabla\Delta\phi_{br,j}^{1G,g} &= \nabla\Delta\rho_{br}^{1G,g} + \lambda_{j} \cdot \nabla\Delta N_{br,j}^{1G,g} + \nabla\Delta \in_{br,j}^{1G,g} \end{aligned} \tag{3}$$

$$\begin{aligned} \nabla\Delta P_{br,j}^{1E,e} &= \nabla\Delta\rho_{br}^{1E,e} + \nabla\Delta\varepsilon_{br,j}^{1E,e} \\ \lambda_{j} \cdot \nabla\Delta\phi_{br,j}^{1E,e} &= \nabla\Delta\rho_{br}^{1E,e} + \lambda_{j} \cdot \nabla\Delta N_{br,j}^{1E,e} + \nabla\Delta \in_{br,j}^{1E,e} \end{aligned} \tag{4}$$

where $\nabla\Delta P_{br,j}^{1G,g}$ denotes the GPS DD code observation; $\nabla\Delta\phi_{br,j}^{1G,g}$ denotes the GPS DD phase observation; $\nabla\Delta\rho_{br,j}^{1G,g}$ denotes the real GPS DD baseline range; $\nabla\Delta N_{br,j}^{1G,g}$ denotes the GPS DD ambiguity; and, $\nabla\Delta\varepsilon_{br,j}^{g,1x}$ and $\nabla\Delta \in_{br,j}^{g,1x}$ are, respectively, the DD unmodeled errors of GPS observation equations. Furthermore, Galileo related parameters in (4) have the same meanings as those in (3).

2.2. Integrated GPS/Galileo Code and Phase Observation Equations

In the construction of multi-system double-differenced equations, it is mainly divided into loosely combined mode (LCM) and tightly combined mode (TCM), which depends on whether each system selects a pivot satellite independently or whether all systems share a common pivot satellite [29].

2.2.1. GPS/Galileo Loosely Combined Mode (LCM)

In GPS/Galileo LCM, one pivot satellite is selected for each system, that is, just as the combination of (3) and (4). Afterwards, the common errors existing in each system can be eliminated by the double difference between the respective systems. In other words, two-times DD processing will be used in the GPS/Galileo combination and the number of observation equations is two less than that of satellites. After further linearization and modularization, (3) and (4) are transformed into:

$$\begin{bmatrix} y^G \\ \\ y^E \end{bmatrix} = \begin{bmatrix} B^G x \\ B^G x + A^G N^G \\ B^E x \\ B^E x + A^E N^E \end{bmatrix} + \begin{bmatrix} \xi^G \\ \\ \xi^E \end{bmatrix} \tag{5}$$

where y is the observation vector consisting of both code and phase observations; x is the vector that contains the increments of the unknown baseline components and B is the corresponding transition matrix; N is the unknown DD integer ambiguity vector and A is the corresponding transition matrix; and, ξ denotes the unmodeled code and phase errors.

2.2.2. GPS/Galileo Tightly Combined Mode (TCM) with Differential Inter-system Biases (DISBs)

Earlier research based on GPS data, when combined with data of the Galileo GIOVE satellites, demonstrated that DISBs are significant between the overlapping observations of L1/E1 and L5/E5a only when different types of receivers are used. DISBs are mainly caused by the different device delay in receivers with respect to different system satellite signals. This means that, if the baseline consists of identical types of receivers, the difference of device delay for different systems can be eliminated by the receiver difference technology. Therefore, DISBs must be taken account of (estimated or offset) when integrated GPS/Galileo data from different types of receivers are used. Assuming that the pivot satellite of both systems belongs to GPS, then, (3) and (4) turn into [25]:

$$\begin{aligned} &\nabla\Delta P_{br,j}^{1G,g} = \nabla\Delta\rho_{br}^{1G,g} + \nabla\Delta\varepsilon_{br,j}^{1G,g} \\ &\lambda_j \cdot \nabla\Delta\phi_{br,j}^{1G,g} = \nabla\Delta\rho_{br}^{1G,g} + \lambda_j \cdot \nabla\Delta N_{br,j}^{1G,g} + \nabla\Delta \in_{br,j}^{1G,g} \\ &\nabla\Delta P_{br,j}^{1G,e} = \nabla\Delta\rho_{br}^{1G,e} + \nabla\Delta d_{br,j}^{1G,e} + \nabla\Delta\varepsilon_{br,j}^{1G,e} \\ &\lambda_j \cdot \nabla\Delta\phi_{br,j}^{1G,e} = \nabla\Delta\rho_{br}^{1G,e} + \lambda_j \cdot \left(\nabla\Delta N_{br,j}^{1G,e} + \nabla\Delta\delta_{br,j}^{1G,e}\right) + \nabla\Delta \in_{br,j}^{1G,e} \end{aligned} \tag{6}$$

where $\nabla\Delta d_{br,j}^{1G,e}$ and $\nabla\Delta\delta_{br,j}^{1G,e}$ denote the code and phase DISBs between the overlapping frequency observations of GPS and Galileo, respectively. After linearization and simplification, (4) is transformed into:

$$\begin{bmatrix} y^G \\ \\ y^{GE} - \delta^{GE} \end{bmatrix} = \begin{bmatrix} B^G x \\ B^G x + A^G N^E \\ B^{GE} x \\ B^{GE} x + A^{GE} N^{GE} \end{bmatrix} + \begin{bmatrix} \xi^G \\ \\ \xi^{GE} \end{bmatrix} \tag{7}$$

where δ^{GE} consists of both the code and phase DISBs between the overlapping frequency observations of GPS and Galileo.

2.2.3. GPS/Galileo Tightly Combined Mode (TCM) without Inter-System Biases (ISBs)

However, the DISBs can be ignored when the combined GPS/Galileo data is collected by identical receivers. Moreover, literature [26] demonstrated that the DISBs between the identical frequencies of GPS and Galileo remain stable, so the introduction of parameter estimation of DISBs in advance can effectively reduce their influence in the positioning solution. Therefore, in the above two cases, (4) and (6) turn into

$$\begin{aligned} \nabla\Delta P_{br,j}^{1G,g/e} &= \nabla\Delta\rho_{br}^{1G,g/e} + \nabla\Delta\varepsilon_{br,j}^{1G,g/e} \\ \lambda_j \cdot \nabla\Delta\phi_{br,j}^{1G,g/e} &= \nabla\Delta\rho_{br}^{1G,g/e} + \lambda_j \cdot \nabla\Delta N_{br,j}^{1G,g/e} + \nabla\Delta \in_{br,j}^{1G,g/e} \end{aligned} \tag{8}$$

After linearization and simplification, we obtain:

$$y^{ge} = \begin{bmatrix} B^{ge}x \\ B^{ge}x + A^{ge}N^{ge} \end{bmatrix} + \xi^{ge} \tag{9}$$

The specific meanings of characters refer to (6). When compared with Formula (4), only one-time DD processing is carried out in the integrated GPS/Galileo baseline resolution in Formula (6). This means that one additional Galileo observation will be preserved as valuable measurement information if the combination of GPS/Galileo TCL was used.

2.3. Stochastic Model

The most traditional and frequently used elevation-dependent weighting model is adopted, which means that the observation of higher elevation satellite tends to have a larger weight and the highest satellite is viewed as the pivot satellite. In this case, the weight of non-differenced observation is defined by

$$q = 1/\sin^2\theta \tag{10}$$

Assuming that $q_r = [q_{1r}\ q_{2r}\ \cdots\ q_{mr}]^T$ and $q_b = [q_{1b}\ q_{2b}\ \cdots\ q_{mb}]^T$ are the $m \times 1$ vectors consisting of all satellites' weights of the rover and base stations excluding the pivot satellite; q_{rp} and q_{bp} are the weights of the pivot satellite with respect to the rover and base stations. Subsequently, the cofactor matrix of single-system DD observation can be expressed as

$$Q = (q_r + q_b) * [1]_m + (q_{rp} + q_{bp}) * I \tag{11}$$

where $[1]_m$ denotes a $m \times m$ matrix full of 1 and I denotes a unit matrix. Afterwards, for a single GPS, the variance–covariance matrix can be derived as:

$$D^G = \begin{bmatrix} \lambda_{Pj}^2 Q^G & I_0 \\ I_0 & \lambda_{\phi j}^2 Q^G \end{bmatrix} \tag{12}$$

where λ_{Pj} and $\lambda_{\phi j}$ denote the code and phase standard deviation with respect to GPS frequency j, respectively; I_0 denotes a 0 square matrix and has the same dimension as Q^G. Subsequently, for GPS/Galileo LCM, the variance–covariance matrix can be transformed into [31]:

$$D^{G/E} = \begin{bmatrix} \lambda_{Pj}^2 Q^G & I_0 & I_0 & I_0 \\ I_0 & \lambda_{Pj}^2 Q^E & I_0 & I_0 \\ I_0 & I_0 & \lambda_{\phi j}^2 Q^G & I_0 \\ I_0 & I_0 & I_0 & \lambda_{\phi j}^2 Q^E \end{bmatrix} \tag{13}$$

For GPS/Galileo TCM with/without ISBs, the variance–covariance can be unified to

$$D^{GE} = \begin{bmatrix} \lambda_{Pj}^2 Q^{GE} & I_0 \\ I_0 & \lambda_{\phi j}^2 Q^{GE} \end{bmatrix} \tag{14}$$

where the dimension of D^{GE} is two less than that of $D^{G/E}$.

2.4. Baseline Length Constraint DD Positioning Method

In deformation monitoring, a priori information of baseline can be used and the baseline length constraint equation is [32]:

$$L = \sqrt{(X_r - X_b)^2 + (Y_r - Y_b)^2 + (Z_r - Z_b)^2} \tag{15}$$

where L is the real baseline length; (X_r, Y_r, Z_r) and (X_b, Y_b, Z_b) are the coordinates of the rover and base receivers, respectively. (15) is linearized at the approximate point (X_r^0, Y_r^0, Z_r^0):

$$L = L_0 + [l\ m\ n] \cdot [\delta x\ \delta y\ \delta z] \tag{16}$$

where $[\delta x\ \delta y\ \delta z] = [X_r, Y_r, Z_r] - [X_r^0, Y_r^0, Z_r^0]$ are the increments of the unknown baseline components in X, Y, and Z directions, respectively. It is worth noting that x in (5) equals $[\delta x\ \delta y\ \delta z]^T$ in (16). $[l\ m\ n]$ are cosine values of baseline increments vector. Subsequently, the integrated GPS/Galileo SFSE DD code and phase observation equations with baseline length constraint can read as:

$$\begin{bmatrix} y^{ge} \\ \\ l_0 \end{bmatrix} = \begin{bmatrix} B^{ge}x \\ B^{ge}x + A^{ge}N^{ge} \\ B_\delta x \end{bmatrix} + \begin{bmatrix} \xi^{ge} \\ \\ 0 \end{bmatrix} \tag{17}$$

where, $l_0 = L - L_0$ is the difference between the real baseline length and its approximate value and B_δ is the coefficient vector $[l\ m\ n]$. Afterwards, the stochastic model for GPS/Galileo TCM with baseline length constraint can be expressed as:

$$D^{GE} = \begin{bmatrix} \lambda_{Pj}^2 Q^{GE} & I_0 & I_0 \\ I_0 & \lambda_{\phi j}^2 Q^{GE} & I_0 \\ I_0 & I_0 & \lambda_{blc}^2 \end{bmatrix} \tag{18}$$

where λ_{blc}^2 denotes the variance of the baseline length.

3. Monitoring Data Collecting for the Forth Bridge

3.1. Data Collecting

At present, the number of long-span bridges across the world is increasing, and extreme weather, including significant temperature fluctuations, strong hurricanes, and earthquakes, continue to damage the structural health of these buildings. Coupled with the increased demand for use, these inevitably accelerate the aging process of structural components. Therefore, it is necessary to conduct a comprehensive assessment of the safety and sustainability for these large bridges during operation. The GeoSHM system, which funded by the European Space Agency, can be employed by the bridge operators to conduct such an assessment. The GeoSHM project is designed as an integrated sensor system that uses GNSS technology integrating low-cost sensors (inertial and inclinometers, etc.) to monitor the deformation of the bridge and ensure the safety and reliability of the bridge operation, whilst using the remote sensing technique to do large scale land stability search. It is divided into five subsystems corresponding to the sensors, data collecting, data processing, bridge structure

assessment, and data management. The project was launched in 2013 and it has been providing long-term monitoring for several bridges in the United Kingdom (UK) and China that include the Forth Road Bridge.

The Forth Road Bridge is located above the Forth River in the north of Edinburgh, Scotland. The bridge is about 2.5 km long and its main span length is 1006 m. In this paper, the Forth Road Bridge is monitored by the GeoSHM project to obtain bridge vibration information. The panorama of the bridge, the distribution of the GNSS sensors, and the bridge coordinate system are shown in Figure 1. Figure 2 shows the pictures of the GNSS stations and their surroundings. Generally, shm1 is set on the north shore of the bridge as the base station, the rover stations shm2 is set in the middle span of the bridge, and shm4 is set at the top of the south tower. Two baselines can then be formed to carry out GNSS relative positioning resolution, which are baseline 1: shm1-shm2 for 1529 m, and baseline 2: shm1-shm4 for 1033 m. Detailed information of the two baselines is provided in Table 1. The receiver types adopted are all Leica GR10 receivers with the antenna of Leica Geosystem GR10 (LEIAR10). The satellite signal frequencies that are adopted here are GPS L1 and Galileo E1. Therefore, in this case, the ISBs between GPS L1 and Galileo E1 can be ignored according to Section 2.2.3. The GPS/Galileo tightly combined mode without inter-system biases will be applied in the baseline resolution. The monitoring data was collected from 1 May to 3 May 2018, with the sampling interval of 10 Hz, and the cutoff angle was set to 10° to reduce the impact of other reflection or refraction signals.

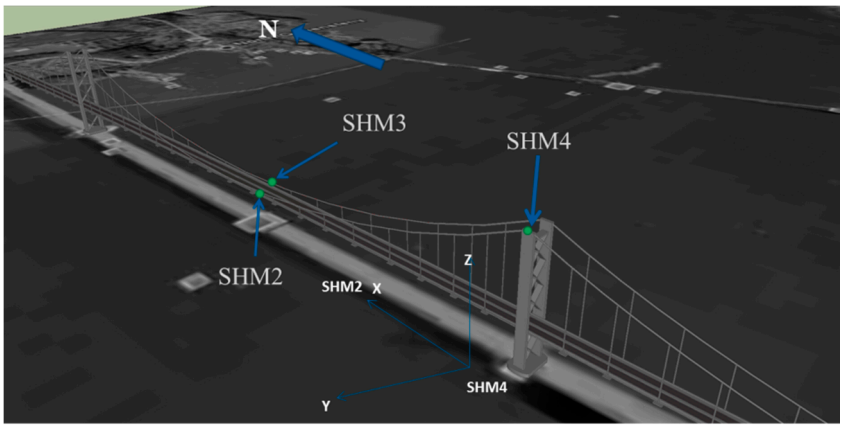

Figure 1. GNSS sensors and coordinate system definition.

Figure 2. The distribution of base stations.

Table 1. The detailed information of the two baselines.

Station	Location	Receiver	Sampling (Hz)	Frequency Band	Baseline	Baseline Length (m)
shm1		Leica GR10	10	L1, E1		
shm2	Middle span	Leica GR10	10	L1, E1	shm1-shm2	1529
shm4	South tower	Leica GR10	10	L1, E1	shm1-shm4	1033

3.2. Sky Plots

Figure 3 shows the sky plots for the various satellites systems at station shm1 on 2 May 2018. The satellite corresponding azimuth and elevation are denoted by the circumference and radii. It can be found that 30 GPS satellites and 14 Galileo satellites can be observed at the station in one day. Because the station is located at 56° north latitude, the GPS and Galileo satellites generally appear in the south of the station and an approximately circular hollow appeared in the north part of each sky plot.

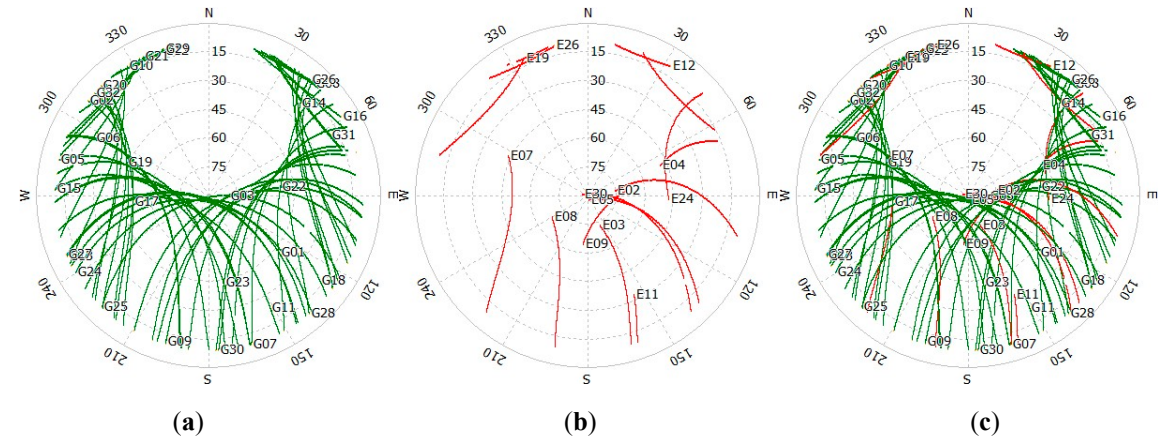

Figure 3. Sky plots (azimuth vs. elevation) for the various satellites systems at station shm1 on 2 May 2018: (**a**) global positioning system (GPS); (**b**) Galileo; and, (**c**) GPS/Galileo.

3.3. Availability and PDOP

In order to reflect the satellite observation condition of the base station, we counted the mean number of visible satellites and the mean value of Position Dilution of Precision (PDOP) under different cutoff angles (ranging from 0° to 40°) during the whole day of 2 May. The corresponding curves can be found in Figure 4a,b. According to the theoretical calculations and experience, the minimum number of satellites that can achieve single point or relative positioning is 4, and good satellite-user geometry corresponds to a PDOP of less than 6. Therefore, these two thresholds evaluate the pass rate of visibility and PDOP (P-num and P-PDOP), and the corresponding curves can be seen in Figure 4c,d. The statistical data of Figure 4 is also shown in Table 2. As the cutoff angle becomes larger, the number of visible satellites decreases, the PDOP increases, and thus the reliability of positioning decreases. For a single GPS system, when the cut-off angle is below 25°, the number of visible satellites can be kept at more than four throughout the day; when the cut-off angle is 30°, the number of satellites is not up to the minimum standard in 4.1% time; when the cut-off angle reaches 40°, the number of satellites in more than half time is insufficient to achieve positioning. Galileo not only has the identical frequency bands as GPS, but also consists of MEO satellites, which ensures strong complementarity between Galileo and GPS—the Galileo satellites can be tracked wherever the GPS satellites are available. Accordingly, Galileo augmenting GPS is an effective and necessary approach to supplement satellites. As we can see from Table 2, the integrated GPS/Galileo has approximately five more satellites than a single GPS when the cutoff angle is below 10°, the number gradually decreases to 2.6 and 1.8 as the cutoff angle increases to 30° and 40°, respectively. The most obvious improvement is the pass rate of

the satellite number—that of GPS/Galileo still keep more than 98.9% under the cutoff angle of 40° and it is better than the single system under the cutoff angle of 30°. From the perspective of PDOP, the improvement is not obvious below 15° cutoff angle (about 0.3–0.4) and it increases to 0.861, 1.863, 2.876, 3.714, and 3.86 as the cutoff angle increases to 20°–40°. At the same time, the PDOP pass rate of GPS/Galileo also improves when compared to that of a single GPS, which is clearly indicated in Figure 4 and Table 2.

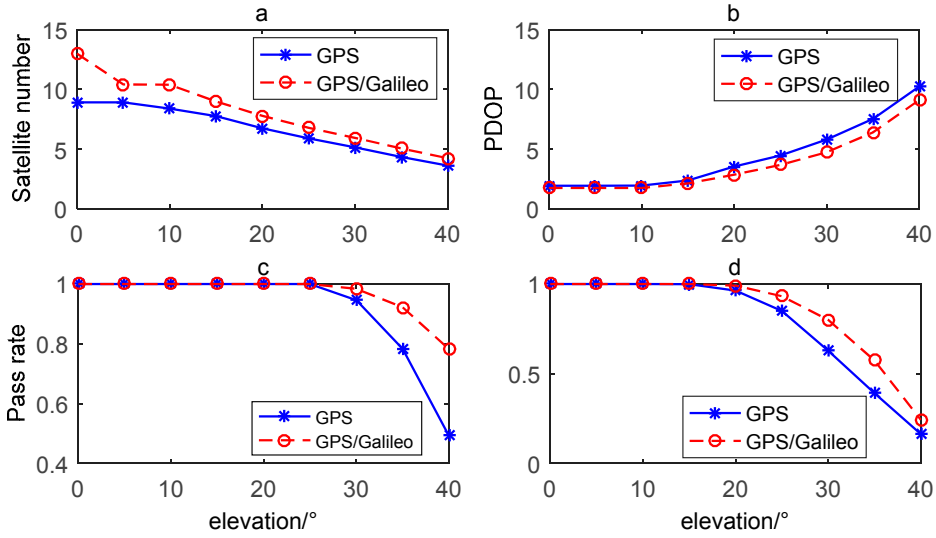

Figure 4. The satellite visibility, Position Dilution of Precision (PDOP), and their pass rate curves of GPS and GPS/Galileo under different cutoff angles (°): (**a**) The satellite visibility; (**b**) PDOP; (**c**) Pass rate of GPS under different cutoff angles (**d**) Pass rate of GPS/Galileo under different cutoff angles.

Table 2. The visibility, PDOP and their pass rate of GPS and GPS/Galileo under different cutoff angles (°).

	elevation/°	**0**	**5**	**10**	**15**	**20**	**25**	**30**	**35**	**40**
GPS	num	12.0	10.6	8.9	7.7	6.7	5.9	5.1	4.4	3.6
	P-num	100%	100%	100%	100%	100%	100%	95.9%	78.7%	44.8%
	PDOP	1.336	1.545	1.883	2.365	3.277	4.929	7.146	10.25	15.19
	P-PDOP	100%	100%	100%	99.6%	96.5%	82.2%	61.5%	39.7%	16.8%
GPS/ Galileo	num	17.7	15.9	13.6	11.6	10.1	8.8	7.7	6.6	5.4
	P-num	100%	100%	100%	100%	100%	100%	100%	100%	98.9%
	PDOP	1.084	1.241	1.48	1.854	2.416	3.063	4.27	6.536	11.3
	P-PDOP	100%	100%	100%	100%	99.5%	98.3%	89.5%	71.7%	30.8%

4. Galileo Augmenting GPS SFSE Precise Positioning Experiment

4.1. Evaluation Index

This section is for the performance evaluation of the two baselines in the different strategies: (a) single GPS, (b) GPS with baseline constraint (C-GPS), (c) GPS/Galileo, and (d) GPS/Galileo with baseline constraint (C-GPS/Galileo). Taking that the bridge vibration may cause the beating of centimeters or even decimeters at any moment into consideration, the addition of constraints at all times will inevitably lead to the correct solution under the vibration condition being affected by the baseline average, so that the result is biased towards the baseline average rather than the true value. Therefore, only if the calculated baseline length differs from the average length by more than a certain degree will the solution will be recalculated with the baseline length constraint.

The following indicators evaluated the experimental results: number of satellites (NOS), PDOP, ADOP, bootstrapped success rate (Bsrt), actual success rate (Asrt), and the baseline precision. The precision of the baseline solution (expressed by the standard deviation) is calculated through a baseline

reference value that is solved by the software RTKLIB. ADOP is an indicator to estimate the accuracy of floating point ambiguity and it can be expressed by [33]:

$$ADOP = \sqrt{|Q_{\hat{a}}|}^{\frac{1}{n}} \tag{19}$$

where $Q_{\hat{a}}$ is the variance–covariance matrix of the float ambiguities and the symbol $||$ denotes the determinants. Bsrt is an indicator for evaluating the success of integer ambiguity resolution and it is expressed as [34].

$$Bsrt = \prod_{i=1}^{n} \left[2\Phi\left(\frac{1}{2\sigma_{\hat{z}_{i|I}}} \right) - 1 \right] \tag{20}$$

where $\sigma_{\hat{z}_{i|I}}$ is the conditional standard deviations of the estimated ambiguities. However, the residual ionosphere, troposphere, or multipath errors in float ambiguities may cause some differences between Bsrt and Asrt [35]. Therefore, Bsrt is a only a theoretical predictive value, not an actual success rate. In view of this, the Asrt will be mainly used to evaluate the correctness of ambiguity resolution and it can be defined as:

$$Asrt = \frac{NOCE}{NOTE} * 100\% \tag{21}$$

where, *NOCE* is the number of correct fixed-ambiguity epochs and *NOTE* is the number of total epochs. It is considered as a correct fixed-ambiguity epoch if the baseline vector that is computed by the fixed integer ambiguities is approximate to the reference value.

4.2. Experiment Analysis

4.2.1. Experiment 1

Figure 5 shows position precision of successful epochs with different strategies for baseline shm1-shm4 and Figure 6 presents the curves of the corresponding NOS, ADOP, and Bsrt. Once the integer ambiguity is fixed incorrectly, the baseline deviation will be up to decimeter level or even worse and is usually not accepted, so the baseline precisions are analyzed only based on the results of successful epochs. The mean NOS, PDOP, ADOP, success rates (both Bsrt and Asrt), and precision of different strategies are presented in Table 3. As we can see, the mean NOS of GPS is 8.8, and for GPS/Galileo, it is about three more. The mean PDOP of GPS and GPS/Galileo is 1.93 and 1.50, respectively. From single GPS to C-GPS/Galileo, the mean ADOP are successively 0.456, 0.389, 0.252, and 0.243. It is obvious that GPS/Galileo and C- GPS/Galileo get better performance in ADOP. For the indicator of Asrt, they are successively 75.01%, 95.10%, 95.47%, and 99.12%. Accordingly, the Asrt of GPS is the worst, that of C-GPS and GPS/Galileo is better and close, and that of C-GPS/Galileo performs best. It is important to note that, for all strategies, Bsrt is much higher than Asrt, especially for single GPS. In terms of precision, both horizontal and vertical precision for the four strategies are very close, and those of the GPS/Galileo combination is only slightly better.

For the single GPS, it is difficult to obtain a high success rate result for baseline resolution, because the number of visible satellites is insufficient—the baseline only has 8.8 common satellites that can only form 7.8 double-differenced equations. Moreover, the height difference between the two ends of the baseline exceeds 100 m, which means that the double-differenced technology may not perfectly eliminate the tropospheric delays. In this condition, the mean Asrt of the single GPS is poor and many interruptions that represent failure epochs appear, as seen in Figure 6a. In view of this, three methods are used to enhance the reliability of positioning and improve the success rate of ambiguity resolution. C-GPS does not increase the number of satellites, thus the PDOP does not change either. Its core idea is to improve the accuracy of the float solution and reduce the search space of the ambiguity by adding the strong constraint of the baseline length, so the ADOP and the Asrt of ambiguity resolution are improved when compared to the case of single GPS. The integrated GPS/Galileo method mainly increases the number of satellites to increase the number of observations, thereby improving the

accuracy of the ambiguity floating point solution, and finally improving the ambiguity resolution success rate. Using this method, the mean ADOP decreases rapidly and the Asrt increases sharply when compared to single GPS. It seems that GPS/Galileo is better than C-GPS, because the ADOP of GPS/Galileo is much better than that of C-GPS. However, it is worth noting that not all-epoch equations have baseline constraints added when C-GPS is adopted. Only if the position deviation of the station exceeds the threshold, the solution will be recalculated with the baseline length constraint, which leads to a smaller ADOP of C-GPS than GPS/Galileo, but their Asrt is similar. It can also be found that C-GPS is more helpful in improving the ambiguity resolution near 16 pm, but GPS/Galileo act around 5 am. This indicates that the combination of the two methods—C-GPS/Galileo may bring about a better baseline resolution effect. From the statistical results, the success rate of the C-GPS/Galileo method is 99.12%, which is the best among the four methods. This indicates that, with the constraints and redundant observations added, the effect of the tropospheric residuals gradually decreases. In addition, since the station shm4 is located at the top of the tower and it is rarely affected by the vibration of the bridge, the horizontal and vertical precision of the baseline solution in the four cases are all about 1 cm. In general, the GPS/Galileo combination method can increase the number of observation equations, and the constraint method can perform a targeted length limitation on the erroneous solution. Although their emphases are different, they are both helpful in improving the precision of float solution and the success rate of ambiguity resolution.

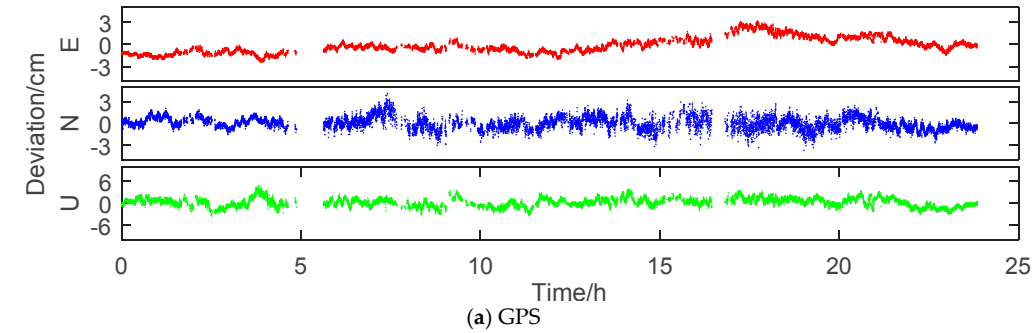

(**a**) GPS

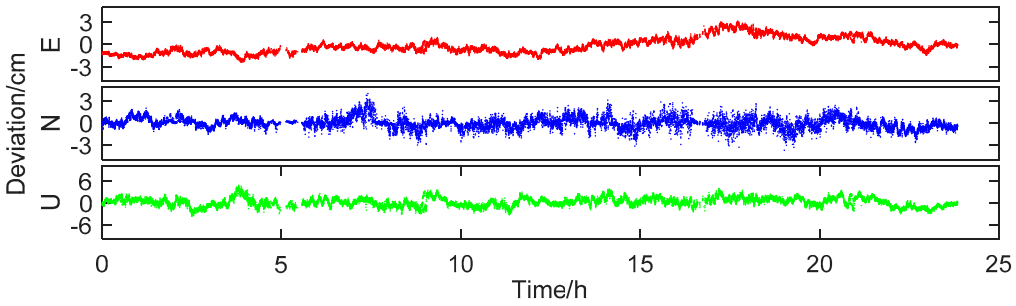

(**b**) GPS+constraint

Figure 5. *Cont.*

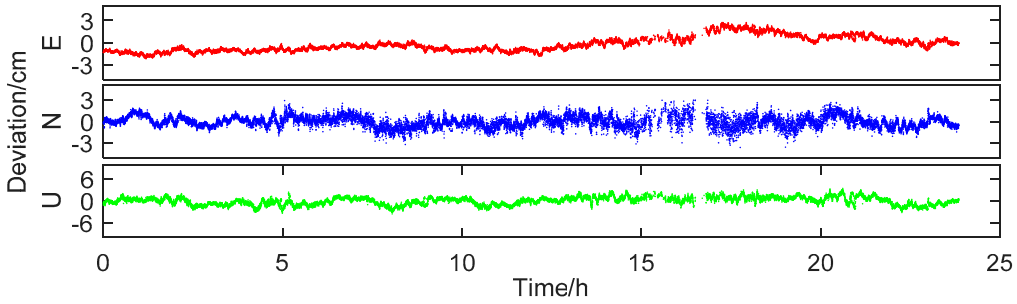

(**c**) GPS+Galileo

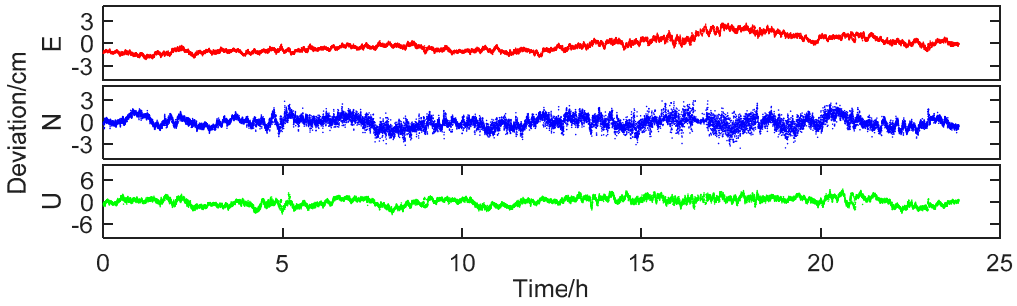

(**d**) GPS+Galileo+constrain

Figure 5. Position deviation of different strategies for baseline shm1-shm4: (**a**) GPS, (**b**) GPS with baseline constraint (C-GPS), (**c**) GPS/Galileo, and, (**d**) C-GPS/Galileo.

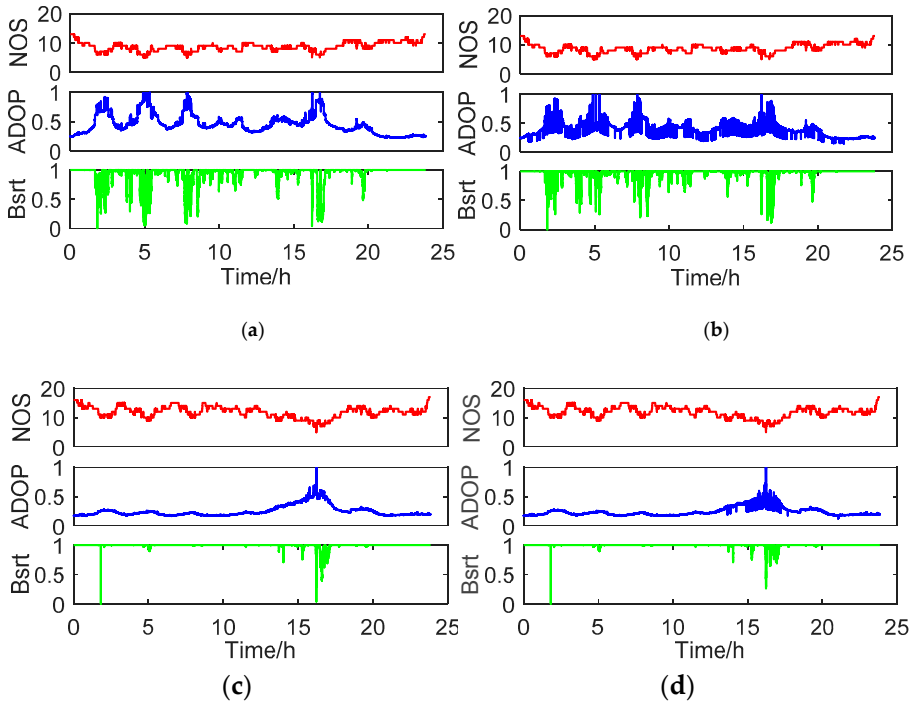

Figure 6. Mean NOS, ADOP, and bootstrapped success rates of different strategies for baseline shm1-shm4: (**a**) GPS, (**b**) C-GPS, (**c**) GPS/Galileo, and (**d**) C-GPS/Galileo.

Table 3. NOS, PDOP, ADOP, success rate and position deviation of different strategies for baseline shm1-shm4.

	NOS	PDOP	ADOP	Asrt	Bsrt	Horizontal Deviation/cm	Up Deviation/cm
GPS	8.8	1.93	0.465	0.7501	0.9363	1.36	1.18
C-GPS	8.8	1.93	0.389	0.9510	0.9709	1.29	1.18
GPS/Galileo	11.9	1.50	0.252	0.9547	0.9919	1.25	1.06
C-GPS/Galileo	11.9	1.50	0.243	0.9912	0.9956	1.25	1.06

4.2.2. Experiment 2

For comparison, we processed another baseline data, of which the rover station is located in the middle span of the bridge, which is the most evident part reflecting the vibration of the bridge. Generally, since the deformation of the bridge is relatively large, the obtained position deviation includes both the random position error and the bias that is caused by the deformation. In the former set of data, since the mobile station is at the most stable position of the bridge, its positional deviation is basically only affected by random noise. However, in this set of data, the position deviation is mainly caused by the vibration and deformation of the bridge. Moreover, the height difference between the two stations is only 18m, which means that the tropospheric delays in this experiment can be ignored. The position deviation of the successful epochs with different strategies for baseline shm1-shm2 is shown in Figure 7, Figure 8 presents the curves of the corresponding NOS, ADOP, and Bsrt, and all evaluation indicators are given in Table 4. Similar to the former baseline, the combination of GPS and Galileo can provide more observational redundancy and increase the precision of the float solution for each epoch; the baseline length constraint method can improve the ambiguity resolution by limiting the baseline length and ambiguity search space for some erroneous epochs. The combination of the two methods will inevitably result in a higher success rate of baseline solution and a more realistic baseline relative position. As we can see from Figure 7, C-GPS improves the Asrt by around 16 pm and GPS/Galileo acts by around 5 am. The Asrt of the two methods are 97.57% and 98.42%, which are 4.33% and 5.18% higher than that of the single GPS. When the C-GPS/Galileo method is adopted, the Asrt of ambiguity resolution is up to 99.76%. This shows that the C-GPS/Galileo method is an effective approach in achieving high accuracy and high success rate baseline resolution in the field of bridge deformation.

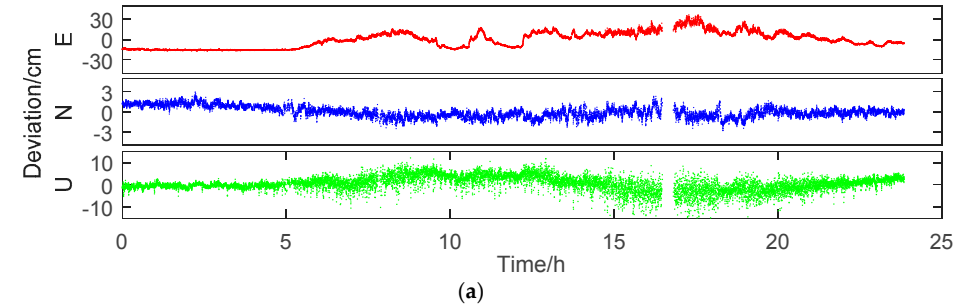

(**a**)

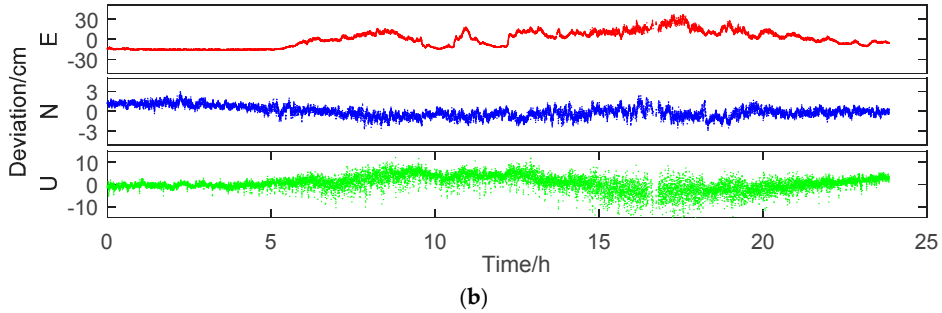

(**b**)

Figure 7. *Cont.*

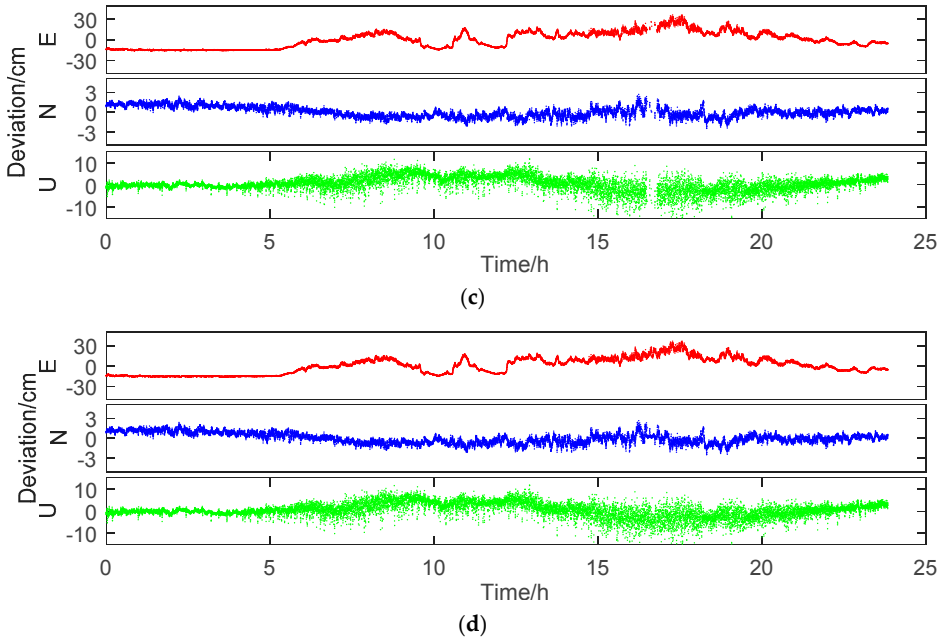

Figure 7. Position deviation of different strategies for baseline shm1-shm2: (**a**) GPS, (**b**) C-GPS, (**c**) GPS/Galileo, and (**d**) C-GPS/Galileo.

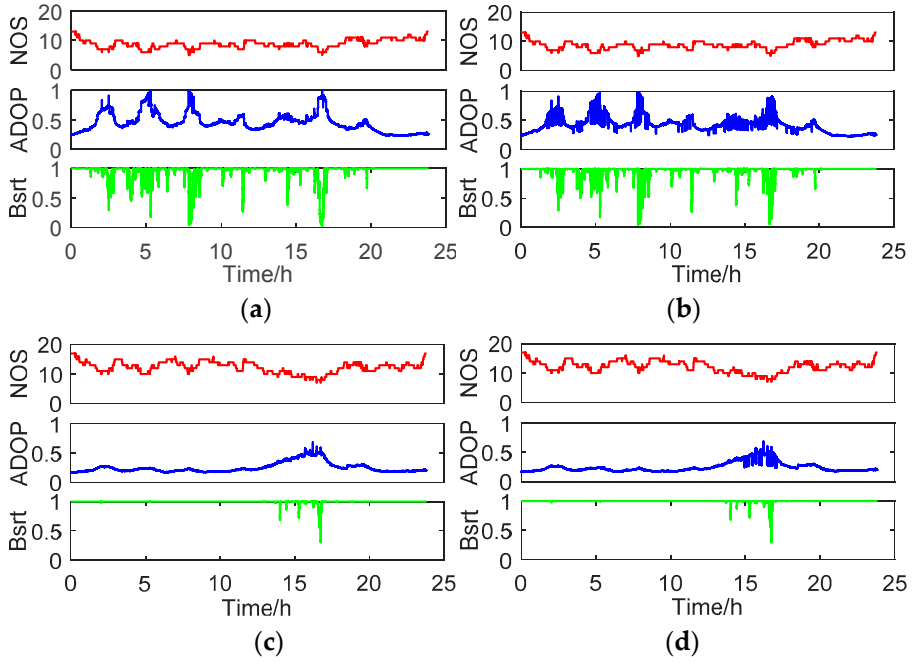

Figure 8. Mean NOS, ADOP, and bootstrapped success rates of different strategies for baseline shm1-shm2: (**a**) GPS, (**b**) C-GPS, (**c**) GPS/Galileo, and (**d**) C-GPS/Galileo.

Table 4. NOS, PDOP, ADOP, success rate and position deviation of different strategies for baseline shm1-shm2.

	NOS	PDOP	ADOP	Asrt	Bsrt	Horizontal Deviation/cm	Up Accuracy/cm
GPS	8.9	1.89	0.453	0.9324	0.9499	11.57	3.23
C-GPS	8.9	1.89	0.437	0.9757	0.9619	11.66	3.24
GPS/Galileo	12.3	1.48	0.250	0.9842	0.9958	11.67	3.17
C-GPS/Galileo	12.3	1.48	0.247	0.9976	0.999	11.78	3.20

In addition, it should be noted that the horizontal deviation of this set of baselines exceeds 1 decimeter, not only far beyond the horizontal deviation of the normal static baseline, but also much larger than the vertical deviation, which should be larger under normal circumstances. This undoubtedly illustrates that the rover station in the middle of the bridge keeps the vibration of the bridge well, and thus this set of data is greatly affected by the vibration of the bridge, especially in the easterly direction, as we can see in Figure 7. Therefore, enhancing the model of the observation equation does not certainly reduce the deviation of the baseline result, which is reflected in Table 4, but it increases the reliability of the ambiguity resolution. Moreover, it is obvious that the Asrt of single GPS in this experiment is about 18% more than that in experiment 1, because the tropospheric residuals in experiment 1 are larger.

The GNSS data is processed in the WGS84 coordinate system, in which the rover station position is described in the form of (X, Y, Z); and, the baseline components (E, N, U) are formed from each monitoring station to the reference station SHM1. These directions are inconsistent with the direction of the vibration component of the bridge. Therefore, a local Bridge Coordinate System (BCS) (XB, YB, ZB) should be defined for further analysis. As shown in Figure 2, the XB axis is formed by shm2 and shm4 and it points to the longitudinal direction of the bridge. Subsequently, YB and ZB correspond to the lateral and height directions. The coordinates in BCS can be obtained by transforming from WGS84 with two-dimensional (2D) similarity transformation. With a baseline solution of shm2 and shm4, the azimuth of the bridge is equal to $0°0'36.36''$, which is so small that it has little effect on the results before and after the conversion. Afterwards, a Fast Fourier Transformation (FFT) algorithm is adopted precisely for detecting the local dominant frequencies of the XB, YB, and ZB direction of station shm4 and shm2 from 15:00 to 16:00, which is resolved by the SFSE GPS/Galileo baseline length constraint model. From Figures 9 and 10, the local dominant frequencies can be identified, which are listed in Table 5 and are consistent with the result in literature [6]. This indicates that the GPS/Galileo with baseline length constraint is an effective approach to monitor the displacement or deflection behavior of bridges.

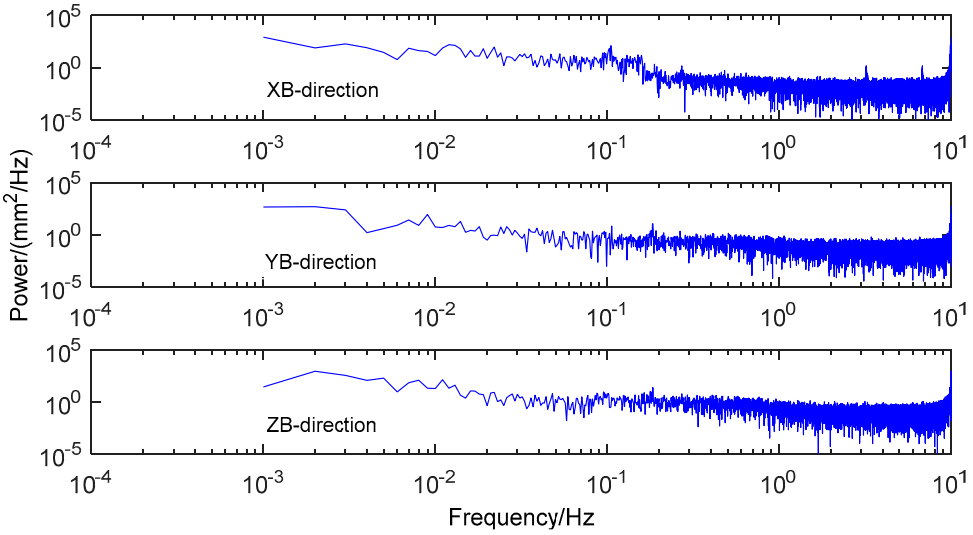

Figure 9. FFT results of shm4.

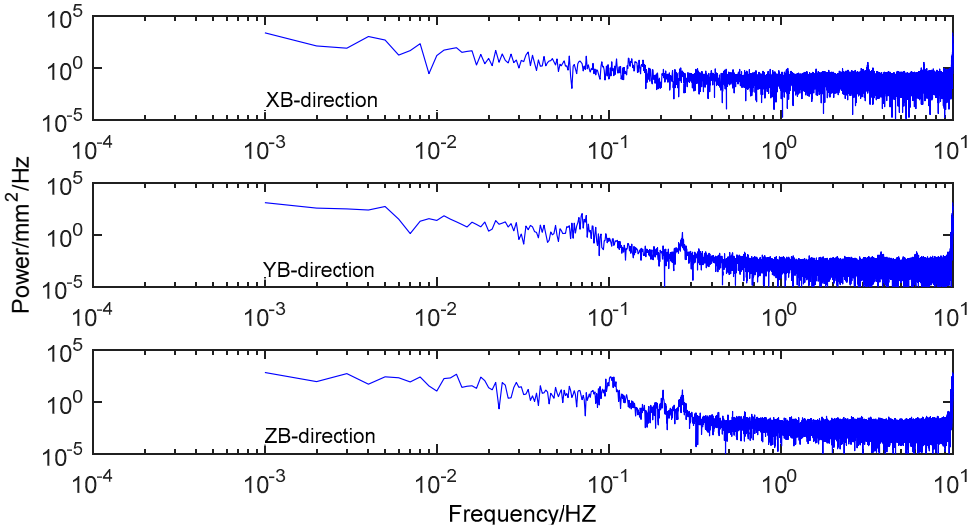

Figure 10. FFT results of shm2.

Table 5. Dominant Frequencies detected from the baseline time series.

Station Name	XB (Longitudinal/Hz)	YB (Lateral/Hz)	ZB (Height/Hz)
Shm2	0.151	0.065 0.268	0.105 0.205 0.268
Shm4	0.105 0.151 0.183	0.183	0.183

5. Conclusions

In this paper, an effective approach to monitor the displacement and deflection behavior of bridges that is called the integrated GPS/Galileo SFSE DD technique with baseline length constraint was introduced. The relative mathematical equations and models, including DD equations, combined modes, weight models, and constraint equations were derived. GNSS receivers monitored the Forth Road Bridge in Scotland to obtain bridge vibration information in order to assess its health condition. Two sets of GPS/Galileo monitoring data that were gathered from this bridge were used for the comparison of the performance of different processing strategies, such as single GPS, GPS with baseline length constraint, integrated GPS/Galileo, and integrated GPS/Galileo with baseline length constraint, respectively. The achieved ambiguity resolution success rates of the four strategies applied to the data set in the first experiment are 75.01%, 95.10%, 95.47%, and 99.12%. For the second experiment, the actual success rates are 93.24%, 97.57%, 98.42%, and 99.76%, which are all higher than the first one. The experimental results showed that integrated GPS/Galileo method can mainly increase the number of observable satellites and hence increasing the number of observations, and the baseline length constraint can improve the accuracy of the float ambiguity. Both of the methods can eventually improve the success rate of ambiguity resolution. In addition, the satellite visibility, PDOP, ADOP, and the baseline precision are also improved by using Galileo data and baseline length constraints. Therefore, integrated GPS/Galileo with a baseline length constraint had the best performance in the two experiments. This also illustrates that a single GPS is difficult to achieve all-weather real-time and high quality bridge deformation monitoring, but by busing Galileo data and baseline length constraints. These issues can be better resolved. In this paper, an FFT method was also used to analyze the bridge position time series that were obtained by GPS/Galileo with constraint. The FFT results are basically consistent with the result that was attained in a previous work.

However, there are still some limitations that need further improvement. Firstly, if the receiver height difference is too large or the water vapor distribution between the rovers on the bridge deck and towers and the base stations is different, then the tropospheric delays cannot be effectively eliminated after double difference. Because of this, the results of experiment 2 are better than that of experiment 1. It is necessary to calculate the tropospheric delay residual while using the water vapor model of the

bridge deck, or estimate it as an unknown parameter during data processing. Secondly, the multipath error is an important factor that cannot be neglected, as it will periodically affect the monitoring results, especially those that are caused by the passing vehicles. We have studied static multipath mitigation in another article, but the corresponding methods are not applicable for dynamic multipath mitigation in the bridge environment. Further spectral analysis methods need to be developed to distinguish the bridge displacement contaminated by white noise and multipath error terms in the observation or coordinate domains. Finally, the Galileo system will be completed in 2020 and it will bring greater improvement in bridge monitoring. The full effect of using Galileo for bridge monitoring needs to be assessed.

Author Contributions: Conceptualization, Q.Z. and C.M.; Methodology, Q.Z. and C.M.; Software, Q.Z. and Y.X.; Validation, Q.Z., C.M. and Y.X.; Formal Analysis, Q.Z., C.M., Y.X. and X.M.; Investigation, Q.Z., L.W., Q.Y. and X.D.; Resources, Q.Z.; Data Curation, Q.Z. and X.M.; Writing-Original Draft Preparation, Q.Z. and C.M.; Writing-Review & Editing, Y.X., P.P. and X.M.; Visualization, Q.Z. and C.M.; Supervision, Q.Z. and X.M.; Project Administration, Q.Z.; Funding Acquisition, Q.Z.

Funding: This research project was jointly supported by National Natural Science Foundation of China (No.41504032, 41811530304), a Project Funded by Science Foundation of Jiangsu Province (No.BK20150175), an International Science And Technology Cooperation Project of Jiangsu Province Government Policy Guidance Plan (BZ2017056) and ESA's GeoSHM project.

Acknowledgments: We thank all the mission scientists and principal investigators who prepared and provided the data used in this study. We also thank the editor and four anonymous reviewers whose comments and suggestions helped to improve the manuscript.

Conflicts of Interest: The authors declare no conflict of interest.

Abbreviations

Abbreviation	Full name
ADOP	ambiguity dilution of precision
Asrt	actual success rate
BCS	Bridge Coordinate System
BDS	BeiDou Satellite Navigation System
Bsrt	bootstrapped success rate
BSSD	between-satellite single-difference
C/N0	carrier-to-noise density ratio
C-GPS	GPS with baseline constraint
C-GPS/Galileo	GPS/Galileo with baseline constraint
DD	double-differenced
DISBs	inter-system biases
FFT	Fast Fourier Transformation
Galileo	Galileo Satellite Navigation System
GeoSHM	The GNSS and Earth Observation for Structural Health Monitoring
GGTO	GPS-to-Galileo Time Offset
GNSS	Global Navigation Satellite System
GPS	Global Positioning System
GPST	GPS Time
GST	Galileo System Time
IOV	In-Orbit Validation
LCM	loosely combined mode
NOS	number of satellites
PDOP	Position Dilution of Precision
PNT	positioning, navigation and timing
P-num	the pass rate of visibility
P-PDOP	the pass rate of PDOP

QZSS	Quasi-Zenith Satellite System
RNP	required navigation performance
RTK	Real-Time Kinematic
SFSE	single-frequency single-epoch
TCM	tightly combined mode

References

1. Yi, T.H.; Li, H.N.; Gu, M. Experimental assessment of high-rate GPS receivers for deformation monitoring of bridge. *Measurement* **2013**, *46*, 420–432. [CrossRef]
2. Yi, T.H.; Li, H.N.; Gu, M. Recent research and applications of GPS based technology for bridge health monitoring. *Sci. China Technol. Sci.* **2010**, *53*, 2597–2610. [CrossRef]
3. Roberts, G.W.; Meng, X.; Dodson, A.H. Integrating a global positioning system and accelerometers to monitor the deflection of bridges. *J. Surv. Eng.* **2004**, *130*, 65–72. [CrossRef]
4. Meng, X.; Dodson, A.H.; Roberts, G.W. Detecting bridge dynamics with GPS and triaxial accelerometers. *Eng. Struct.* **2007**, *29*, 3178–3184. [CrossRef]
5. Psimoulis, P.A.; Stiros, S.C. A supervised learning computer-based algorithm to derive the amplitude of oscillations of structures using noisy GPS and robotic theodolites (RTS) records. *Comput. Struct.* **2012**, *92*, 337–348. [CrossRef]
6. Meng, X.; Xi, R.; Xie, Y. Dynamic characteristic of the forth road bridge estimated with GeoSHM. *J. Glob. Position Syst.* **2018**, *16*, 4–18. [CrossRef]
7. Meng, X.; Nguyen, D.T.; Xie, Y.; Owen, J.S.; Psimoulis, P.; Ince, S.; Chen, Q.; Ye, J.; Bhatia, P. Design and implementation of a new system for large bridge monitoring-GeoSHM. *Sensors* **2018**, *18*, 775. [CrossRef] [PubMed]
8. Xi, R.; Jiang, W.; Meng, X.; Chen, H.; Chen, Q. Bridge monitoring using BDS-RTK and GPS-RTK techniques. *Measurement* **2018**, *120*, 128–139. [CrossRef]
9. Liu, X.; Zhang, S.; Zhang, Q.; Yang, W. An extended ADOP for performance evaluation of single-frequency single-epoch positioning by BDS/GPS in Asia-Pacific region. *Sensors* **2017**, *17*, 2254. [CrossRef] [PubMed]
10. Shi, C.; Zhao, Q.L.; Min, L.; Tang, W.M.; Hu, Z.G.; Lou, Y.D.; Zhang, H.P.; Niu, X.J.; Liu, J.N. Precise orbit determination of Beidou satellites with precise positioning. *Sci. China Earth Sci.* **2012**, *55*, 1079–1086. [CrossRef]
11. Zhang, Q.; Yang, W.; Zhang, S.; Yao, L. Performance Evaluation of QZSS Augmenting GPS and BDS Single-Frequency Single-Epoch Positioning with Actual Data in Asia-Pacific Region. *ISPRS Int. J. Geo-Inf.* **2018**, *7*, 186. [CrossRef]
12. Yalvac, S.; Berber, M. Galileo satellite data contribution to GNSS solutions for short and long baselines. *Measurement* **2018**, *124*, 173–178. [CrossRef]
13. Ochieng, W.Y.; Sauer, K.; Cross, P.A.; Sheridan, K.F.; Iliffe, J.C.; Lannelongue, S.; Ammour, N.; Petit, K. Potential performance levels of a combined Galileo/GPS navigation system. *J. Navig.* **2001**, *54*, 185–197. [CrossRef]
14. Cederholm, P. PDOP values for simulated GPS/Galileo positioning. *Emp. Surv. Rev.* **2013**, *38*, 218–228. [CrossRef]
15. Zhao, C.; Ou, J.; Yuan, Y. Positioning accuracy and reliability of Galileo, integrated GPS-Galileo system based on single positioning model. *Chin. Sci. Bull.* **2005**, *50*, 1252–1260. [CrossRef]
16. O'Keefe, K.; Julien, O.; Cannon, M.E.; Lachapelle, G. Availability, accuracy, reliability, and carrier-phase ambiguity resolution with Galileo and GPS. *Acta Astronaut.* **2006**, *58*, 422–434. [CrossRef]
17. Tsakiri, M. Evaluation of GPS/Galileo rtk network configuration: Case study in Greece. *J. Surv. Eng.* **2011**, *53*, 156–166. [CrossRef]
18. Cai, C.; Luo, X.; Liu, Z.; Xiao, Q. Galileo signal and positioning performance analysis based on four IOV satellites. *J. Navig.* **2014**, *67*, 810–824. [CrossRef]
19. Paziewski, J.; Wielgosz, P. Assessment of GPS + Galileo and multi-frequency Galileo single-epoch precise positioning with network corrections. *GPS Solut.* **2014**, *18*, 571–579. [CrossRef]
20. Chu, F.Y.; Yang, M. GPS/Galileo long baseline computation: Method and performance analyses. *GPS Solut.* **2014**, *18*, 263–272. [CrossRef]

21. Dennis, O.; Arora, B.S.; Teunissen, P.J.G. Predicting the success rate of long-baseline GPS+Galileo (partial) ambiguity resolution. *J. Navig.* **2014**, *67*, 385–401.
22. Afifi, A.; Elrabbany, A. Performance analysis of several GPS/Galileo precise point positioning models. *Sensors* **2015**, *15*, 14701–14726. [CrossRef] [PubMed]
23. Siejka, Z. Validation of the Accuracy and Convergence Time of Real Time Kinematic Results Using a Single Galileo Navigation System. *Sensors* **2018**, *18*, 2412. [CrossRef] [PubMed]
24. Paziewski, J.; Wielgosz, P. Accounting for Galileo–GPS inter-system biases in precise satellite positioning. *J. Geod.* **2015**, *89*, 81–93. [CrossRef]
25. Odijk, D.; Teunissen, P.J.G. Characterization of between-receiver GPS-Galileo inter-system biases and their effect on mixed ambiguity resolution. *GPS Solut.* **2013**, *17*, 521–533. [CrossRef]
26. Paziewski, J.; Sieradzki, R.; Wielgosz, P. Selected properties of GPS and Galileo-iov receiver intersystem biases in multi-GNSS data processing. *Meas. Sci. Technol.* **2015**, *26*, 095008. [CrossRef]
27. Odolinski, R.; Teunissen, P.J.G.; Odijk, D. Combined BDS, Galileo, QZSS and GPS single-frequency RTK. *GPS Solut.* **2015**, *19*, 151–163. [CrossRef]
28. Quan, Y.; Lau, L.; Roberts, G.W. Measurement Signal Quality Assessment on All Available and New Signals of Multi-GNSS (GPS, GLONASS, Galileo, BDS, and QZSS) with Real Data. *J. Navig.* **2016**, *69*, 313–334. [CrossRef]
29. Zhang, X.; Wu, M.; Liu, W. BeiDou B2/Galileo E5b Short Baseline Tight Combination Relative Positioning Model and Performance Evaluation. *Acta Geoda Sin.* **2016**, *45*, 1–11.
30. Hahn, J.H.; Powers, E.D. Implementation of the GPS to Galileo time offset (GGTO). In Proceedings of the 2005 IEEE International Frequency Control Symposium and Exposition, Vancouver, BC, Canada, 29–31 August 2005. [CrossRef]
31. Deng, C.; Tang, W.; Liu, J.; Shi, C. Reliable single-epoch ambiguity resolution for short baselines using combined GPS/BeiDou system. *GPS Solut.* **2014**, *18*, 375–386. [CrossRef]
32. Liu, X.; Chen, G.; Zhang, Q.; Zhang, S. Improved single-epoch single-frequency par lambda algorithm with baseline constraints for the Beidou navigation satellite system. *IET Radar Sonar Navig.* **2017**, *11*, 1549–1557. [CrossRef]
33. Teunissen, P.J.G. A canonical theory for short GPS baselines. Part iv: Precision versus reliability. *J. Geod.* **1997**, *71*, 513–525. [CrossRef]
34. Teunissen, P.J.G. Success probability of integer GPS ambiguity rounding and bootstrapping. *J. Geod.* **1998**, *72*, 606–612. [CrossRef]
35. Liu, J.; Deng, C.; Tang, W. Review of GNSS ambiguity validation theory. *Geomat. Inf. Sci. Wuhan Univ.* **2014**, *39*, 1009–1016.